Boundary-Layer Meteorol (2012) 145:131–143
DOI 10.1007/s10546-011-9683-4

ARTICLE

Observation of a Self-Limiting, Shear-Induced Turbulent Inversion Layer Above Marine Stratocumulus

J. Katzwinkel · H. Siebert · R. A. Shaw

Received: 16 August 2011 / Accepted: 28 November 2011 / Published online: 18 December 2011

Abstract High-resolution measurements of thermodynamic, microphysical, and turbulence properties inside a turbulent inversion layer above a marine stratocumulus cloud layer are presented. The measurements are performed with the helicopter-towed measurement payload Airborne Cloud Turbulence Observation System (ACTOS), which allows for sampling with low true air speeds and steep profiles through cloud top. Vertical profiles show that the turbulent inversion layer consists of clear air above the cloud top, with nearly linear profiles of potential temperature, horizontal wind speed, absolute humidity, and concentration of interstitial aerosol. The layer is turbulent, with an energy dissipation rate nearly the same as that in the lower cloud, suggesting that the two are actively coupled, but with significant anisotropic turbulence at the large scales within the turbulent inversion layer. The turbulent inversion layer is traversed six times and the layer thickness is observed to vary between 37 and 85 m, whereas the potential temperature and horizontal wind speed differences at the top and bottom of the layer remain essentially constant. The Richardson number therefore increases with increasing layer thickness, from approximately 0.2 to 0.7, suggesting that the layer develops to the point where shear production of turbulence is sufficiently weak to be balanced by buoyancy suppression. This picture is consistent with prior numerical simulations of the evolution of turbulence in localized stratified shear layers. It is observed that the large eddy scale is suppressed by buoyancy and is on the order of the Ozmidov scale, much less than the thickness of the turbulent inversion layer, such that direct mixing between the cloud top and the free troposphere is inhibited, and the entrainment velocity tends to decrease with increasing turbulent inversion-layer thickness. Qualitatively, the turbulent inversion layer likely grows through nibbling rather than engulfment.

J. Katzwinkel (✉) · H. Siebert
Leibniz Institute for Tropospheric Research, Permoserstraße 15, 04318 Leipzig, Germany
e-mail: jeannine.katzwinkel@tropos.de

H. Siebert
e-mail: siebert@tropos.de

R. A. Shaw
Department of Physics, Michigan Technological University, 1400 Townsend Drive, Houghton, MI 49931, USA
e-mail: rashaw@mtu.edu

Keywords Cloud-top entrainment · Stratiform boundary-layer cloud

1 Introduction

The cloud-topped marine boundary layer is often strongly decoupled from the overlying troposphere. The interface is typically characterized by sharp, vertical gradients in potential temperature, absolute humidity, aerosol concentration, and often horizontal wind velocity. So compared to the free troposphere, the boundary layer tends to be relatively cold and humid, with rather distinct dynamical and pollution properties. The temperature inversion acts to suppress mixing but what little turbulence forms results in important coupling between the boundary layer and the troposphere, and the resulting entrainment is critical to cloud-layer evolution at the boundary-layer top (e.g., Stevens 2002). Generally, turbulence at the interface is thought to be generated through thermodynamic destabilization, for example due to radiative cooling and possible buoyancy reversal (e.g., Deardorff 1980; Mellado 2010), or through wind shear and the resulting Kelvin–Helmholtz instability (e.g., Wang et al. 2008). Formation of turbulence and the evolution of turbulent mixing in a stably stratified environment are problems of broad geophysical interest, and have been widely explored. Generally speaking, in flows with constant shear and density gradients the growth of turbulent kinetic energy is inhibited by buoyancy forces for Richardson numbers greater than approximately 0.1 (Peltier and Caulfield 2003). Buoyancy fundamentally alters (tending to suppress) the turbulence at scales on the order of or greater than the Ozmidov scale, and for flows with spatially localized shear and stratification, such as often exists at stratocumulus cloud top, this length scale is expected to decrease with time as mixing progresses (Smyth and Moum 2000). Such layers have been observed to grow to an asymptotic thickness as the shear contribution to the turbulent kinetic energy budget decays more rapidly than the buoyancy contribution of opposite sign (Smyth and Moum 2000; Brucker and Sarkar 2007). This interplay of destabilizing shear and stabilizing buoyancy is made further complex when the interface is bounded on one side by a cloud layer, leading to radiative and evaporative energy fluxes that tend to alter the energy budget and therefore the rate of turbulent mixing.

What is the nature of the cloud-top environment? Lenschow et al. (2000) showed through an analysis of Dynamics and Chemistry of the Marine Stratocumulus (DYCOMS; Lenschow et al. 1988) data that the cloud/clear air transition is very sharp, but also that the interface is "leaky", leading to a mixture of boundary-layer and free tropospheric air just above cloud top. In these studies there was very little vertical shear and we may ask, therefore, to what extent the leakiness depends on shear. Rogers and Telford (1986) observed one case with appreciable vertical shear in which a clearly defined, 10–15-m thick transition layer formed between cloud top and the inversion. They argued that the layer acts as a buffer against entrainment instability: direct mixing between cloud and the free troposphere would support the instability, but mixing across the entire transition layer is damped. Large-eddy simulation (LES) demonstrates that this conditioned layer is almost always present above stratocumulus cloud tops and that its maintenance is related to 'local' shear effects due to convective eddies (Moeng et al. 2005). High spatial resolution measurements have provided further characterization of what has been termed the "entrainment interface layer," consisting of filaments of clear and cloudy air over a wide range of sizes down to the instrument resolution of 0.1 m (Gerber et al. 2005; Haman et al. 2007). Based on those measurements it was suggested that after multiple mixing events the entrainment interface layer becomes conditioned to the extent that there is near buoyancy match with the air at cloud top (Gerber et al. 2005). de Roode and Wang (2007) provide further observational evidence from FIRE I

and refer to the process as detrainment, through which diluted, but still saturated air, forms a local environment at the cloud boundary. The dependence of the interface layer on shear was highlighted in the LES studies of Wang et al. (2008), who observed that the layer thickness increases with shear intensity, and, consistent with the cloud-free work described in the previous paragraph, noted that the inversion layer tends to evolve to a constant bulk Richardson number of approximately 0.3.

We report here on observations of the turbulent and thermodynamic structure of a stratocumulus-cloud-topped marine boundary layer under conditions of relatively strong wind shear. The dataset is unique because of the full range of turbulence, thermodynamic, and microphysical measurements, obtained at high spatial resolution and with spatially collocated instruments to within a fraction of a metre; it therefore provides a detailed view into the relatively sharp turbulent inversion layer (TIL) at cloud top. The measurements were obtained using the helicopter-borne measurement payload Airborne Cloud Turbulence Observation System (ACTOS).

2 Experimental

In October 2007 measurements were performed in a marine stratocumulus layer above the Baltic Sea near Kiel, Germany with the helicopter-borne measurement payload ACTOS. ACTOS is attached to the helicopter by means of a 140 m long rope to avoid any influence from the rotor downwash and its typical true airspeed is about 15 m s^{-1} enabling high-resolution measurements in the cloudy atmosphere. A detailed description of the ACTOS payload and its general performance is given in Siebert et al. (2006a). The analysis of this work is mainly based on measurements of the three-dimensional wind vector measured with an ultra-sonic anemometer (hereafter called "sonic"), Solent HS (Gill Instruments, Lymington, UK), the liquid water content (LWC) measured with a particle volume monitor (PVM-100A; Gerber et al. 1994), the temperature (T) measured with a special cloud thermometer (Ultra-Fast Thermometer, UFT, Haman et al. 1997), the absolute humidity (a) measured with an open-pass infrared absorption hygrometer (Licor, LI-7500) and the number concentration of interstitial aerosol (N) measured with a condensation particle counter (CPC, model 3762A, TSI Inc., St. Paul, Minnesota, USA). A comprehensive description of the measurement equipment can be found in Siebert et al. (2003).

3 Observations and Data Analysis

The following analysis is based on a single flight from October 8, 2007, performed between 0930 and 1100 UTC. The marine boundary layer had a thickness of 1.3 km. After vertical profiling, ACTOS performed six "dolphin-like" profiles, a sinusoidal flight pattern in and out of cloud top and the TIL with a vertical peak-to-peak amplitude of approximately 300 m. Selected parameters of this record are presented in Fig. 1. The sampling strategy is illustrated by means of the measurement height (z) shown in panel (a), the cloud is indicated by the LWC in panel (b), liquid water potential temperature ($\Theta_l = \Theta - \frac{L_v}{c_p} q_l$, where L_v is the latent heat of vaporization, c_p is the specific heat at constant pressure of air, and q_l is the liquid water mixing ratio) and the absolute humidity a are shown in panel (c), and the horizontal wind velocity (U) and the particle number concentration of interstitial aerosol N are presented in panel (d).

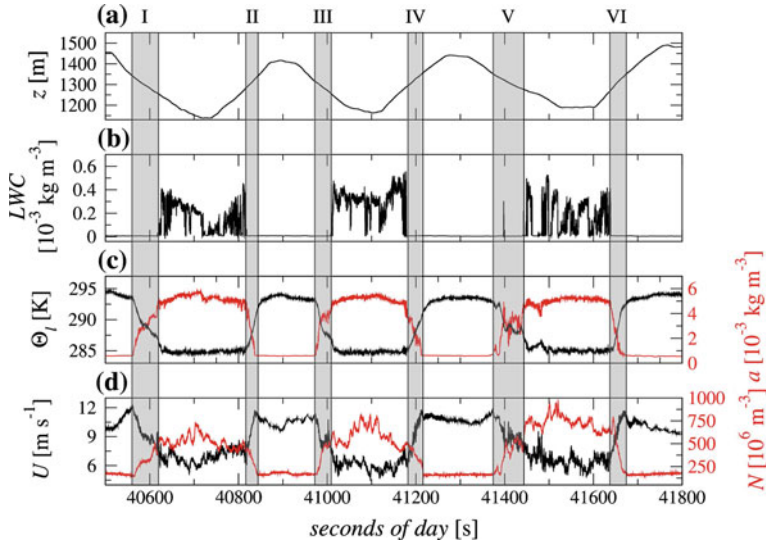

Fig. 1 Time series of six subsequent profiles at the top of a marine stratocumulus layer. The following data are shown: **a** height (z), **b** LWC, **c** liquid water potential temperature (Θ_l) in *black* and absolute humidity (a) in *red*, **d** horizontal wind velocity (U) in *black* and number concentration of interstitial aerosol (N) in *red*. The mean true airspeed of ACTOS was $14\,\mathrm{m\,s^{-1}}$. The *grey boxes* mark the respective TIL of each profile

The cloud layer is characterized by a maximum $LWC \approx 0.4 \times 10^{-3}\,\mathrm{kg\,m^{-3}}$, a mean $\Theta_l \approx 285\,\mathrm{K}$ and $a \approx 5 \times 10^{-3}\,\mathrm{kg\,m^{-3}}$. The particle number concentration N inside the cloud layer fluctuates between 500×10^6 and $900 \times 10^6\,\mathrm{m^{-3}}$. The free troposphere above the cloud is characterized by $\Theta_l \approx 293\,\mathrm{K}$, $a \approx 0.7 \times 10^{-3}\,\mathrm{kg\,m^{-3}}$ and a nearly constant $N \approx 150 \times 10^6\,\mathrm{m^{-3}}$. In between, the vertical shaded regions mark the TIL, which is characterized by a strong wind shear, where U increases from $6\,\mathrm{m\,s^{-1}}$ inside the cloud layer to $11\,\mathrm{m\,s^{-1}}$ in the free atmosphere and all other parameters gradually change from their in-cloud values to the free troposphere.

Figure 2 shows a more detailed view of the turbulent and thermodynamic properties for one penetration through the TIL (transit IV in Fig. 1). The first four panels (Fig. 2a–d) display LWC, Θ_l, a, U, and N. In the following three panels (Fig. 2e–g) the turbulence is characterized by means of the gradient Richardson number Ri, the local turbulent energy dissipation rate ε_τ, and the ratio of the variances of the transverse and longitudinal components of velocity σ_w^2/σ_u^2. The gradient Richardson number describes the ratio between turbulence production by wind shear and the damping effect due to atmospheric stability, viz.

$$Ri = \frac{g}{\Theta_l} \frac{\frac{\mathrm{d}\Theta_l}{\mathrm{d}z}}{\left(\frac{\mathrm{d}U}{\mathrm{d}z}\right)^2}. \tag{1}$$

Kondo et al. (1978) pointed out that for $Ri < 0.2$ the flow is fully turbulent, and as $Ri \approx 1$ is approached the turbulence decreases and becomes more intermittent, and finally when $Ri > 1$ turbulence is strongly damped due to the stable stratification. A critical value of $Ri_c = 1$ is marked with a vertical black line in Fig. 2e. In practice, the gradient Richardson number Ri is calculated from differences in U and Θ over a height difference of 5 m, and then smoothed with a 25-m vertical running average. The local energy dissipation rate ε_τ describes the energy dissipation for non-overlapping sub-records of length τ; here,

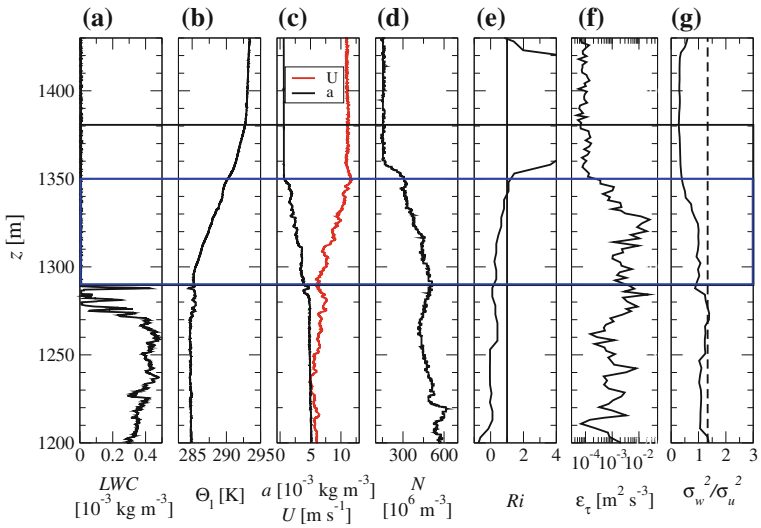

Fig. 2 Vertical profiles of: **a** LWC, **b** liquid water potential temperature (Θ_l), **c** absolute humidity (a) in *black* and horizontal wind velocity (U) in *red*, **d** number concentration of interstitial aerosol (N), **e** gradient Richardson number (Ri), with $Ri = 1$ marked with the *vertical black line*, **f** local energy dissipation rate (ε_τ) and **g** local isotropy (σ_w^2/σ_u^2), with $\sigma_w^2/\sigma_u^2 = 4/3$ marked with the *vertical dotted line*. The *horizontal blue lines* denote the TIL, as defined by the level at which $Ri = 1$. For this example the inversion layer extends somewhat higher than the interfacial layer. The profile corresponds to IV in Fig. 1

$\tau = 1$ s is chosen, which corresponds to a horizontal flight path of about 15 m (approximately 2 m in the vertical direction). For every sub-record, the second-order structure function $S^{(2)}(t') \equiv \left\langle \left(u(t) - u(t+t')\right)^2 \right\rangle_\tau \simeq 2\varepsilon_\tau^{2/3} \left(t' \langle u \rangle_\tau\right)^{2/3}$ is estimated, where the brackets denote an average over time τ and u is the longitudinal wind component of the wind-velocity vector. From this equation, for every sub-record ε_τ is derived. A more detailed discussion of this method is described in Siebert et al. (2006b) and references therein. The last panel (Fig. 2g) presents the ratio of σ_w^2/σ_u^2 as a measure of local isotropy of the velocity field, where each value is estimated from a sub-record of the same length as for ε_τ. The ratio of the one-dimensional power spectra of the transversal to longitudinal velocity components tends to 4/3 for small scales indicating local isotropy (see Wyngaard 2010 for example). Since the variance equals the integrated power spectrum, the 4/3 ratio is also valid for the variances. However, it has to be pointed out that the lower integration limit is determined by the length of the sub-record and, therefore, σ_u^2 and σ_w^2 do not represent the entire layer and contributions from larger structures are filtered out. In this work we use this measure in a qualitative way to distinguish between the different behaviour in the cloud and the TIL. Observations in the atmosphere reveal ratios in the range 1–4/3 (Biltoft 2001).

The vertical profiles in Fig. 2 illustrate the remarkably linear transition from boundary layer to free-troposphere values of a, U, and N. Interestingly, in this profile the inversion layer (Θ_l) actually extends slightly higher into the troposphere (as is the case with four of the other six profiles shown in Fig. 1). The blue horizontal lines in Fig. 2 denote the TIL, as defined primarily through the wind shear, and to a lesser extent through the absolute humidity. Panels e and f show that the TIL is characterized by Ri slightly less than 1, and approximately constant ε_τ at about the same levels as in the underlying cloud layer. A difference between the cloud layer and the TIL is clearly seen in the local isotropy ratio shown in panel (g). While

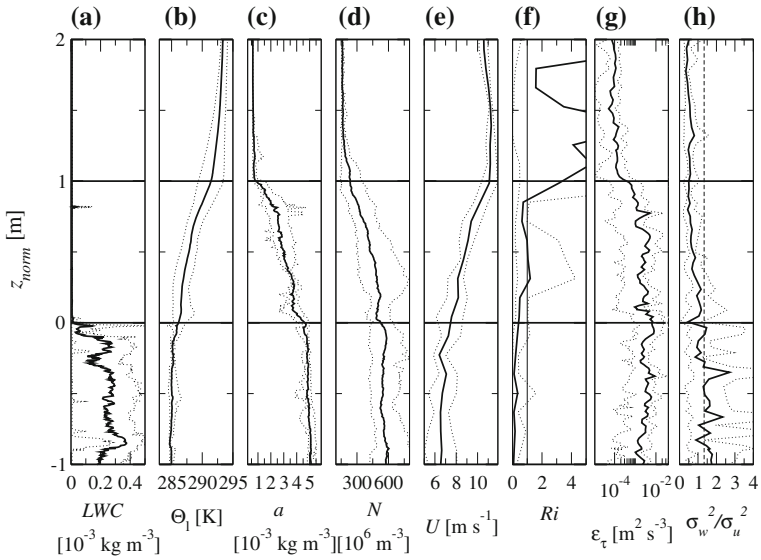

Fig. 3 Mean profiles averaged over six individual soundings. Before averaging, the height was normalized with $z_{\mathrm{norm}} = 0$ denoting the height of cloud top and $z_{\mathrm{norm}} = 1$ marking the height of disappearance of the horizontal wind shear. The *black lines* represent the averaged values and the *dotted lines* mark the minimum and maximum values for the six profiles. Displayed are: **a** LWC, **b** liquid water potential temperature (Θ_{l}), **c** absolute humidity (a), **d** number concentration of interstitial aerosol (N), **e** horizontal wind velocity (U), **f** gradient Richardson number (Ri), **g** local energy dissipation rate (ε_τ) and **h** local isotropy, with $\sigma_{\mathrm{w}}^2/\sigma_{\mathrm{u}}^2 = 4/3$ marked with the *vertical dotted line*

inside the cloud layer the turbulence tends to be isotropic, the ratio decreases significantly below unity inside the TIL representing anisotropy and increasingly two-dimensional turbulence. It should be noted that this departure from isotropy casts some doubt on the precise estimates of ε_τ because the connection to the second-order structure function (described in the previous paragraph) assumes homogeneous, isotropic turbulence (Siebert et al. 2009).

In order to obtain a more generalized picture of the cloud top and the TIL, the thermodynamic and turbulent properties are averaged over the six profiles. To accomplish the averaging the height was normalized according to the following two definitions: $z_{\mathrm{norm}} = 0$ denotes the cloud top and $z_{\mathrm{norm}} = 1$ marks the top of the TIL. The averaged profiles are shown in Fig. 3 and display similar qualitative structure as in the single profiles. The black lines represent the mean values and the dotted lines denote the maximum and minimum values of each parameter.

All averaged variables are nearly constant with height within the observed regions above and below the TIL, i.e., inside the cloud and in the free troposphere. In between lies the well-defined TIL, which covers nearly the whole inversion layer and acts as a turbulent entrainment region between the two bounding thermodynamic and dynamic regimes. Specifically, variables Θ_{l}, a, U, and N change nearly linearly across the TIL from cloud to free tropospheric values. At the same time, ε_τ is essentially uniform across the cloud and the inversion layer, suggesting that the two are strongly coupled dynamically: $\varepsilon_\tau \sim 10^{-3}\,\mathrm{m^2\,s^{-3}}$ is observed both in the cloud and in the TIL and decreases by nearly one order of magnitude at the top of the TIL. This is consistent with the Richardson number, which is below unity for the cloud and TIL and sharply increases at the boundary between the TIL and the free troposphere. However, the small-scale structure of the turbulence in the cloud and the TIL

differs significantly in terms of isotropy. Due to the strong stratification inside the TIL, the turbulence tends to become more anisotropic and two-dimensional, which is typical for stably stratified flows (Mauritsen et al. 2007).

4 Discussion

The porpoise-dive sampling strategy is often used in aircraft studies of marine stratocumulus cloud tops. For example, during the DYCOMS-II experiment (e.g., Haman et al. 2007) a similar approach led to the estimate of an entrainment interface layer from 0 to 70 m thick, based on high-resolution LWC and temperature measurements. It is important to recognize, however, that the ACTOS profiles should be interpreted somewhat differently because of the relative flight speeds. The true airspeed of the C-130 aircraft is about $100\,\mathrm{m\,s^{-1}}$ with a climbing rate of about $2\,\mathrm{m\,s^{-1}}$. Consequently, the aspect ratio of vertical to horizontal flight path is about 1:50 compared to 1:7 for the ACTOS flights. Therefore, the slant path taken through the TIL with the C-130 is much more influenced by large-scale horizontal variability and the measurements tend to represent an averaged picture of the cloud top, even for single profiles. In contrast, in the ACTOS sampling scenario the slant path is considerably less than the depth of the boundary layer ($\approx$1,300 m), so it does approximate a 'vertical profile' by avoiding averaging over many boundary-layer scales.

The consistent picture of the TIL emerges in spite of significant variability observed in the layer thickness. The observed thickness Δz_{sub} of the TIL ranges from 37 to 85 m, between the nearly constant tropospheric and cloud values for liquid water potential temperature, $\Theta_{\mathrm{l,top}} = 293$ and $\Theta_{\mathrm{l,cloud}} = 285\,\mathrm{K}$, and horizontal wind speed $U_{\mathrm{top}} = 11\,\mathrm{m\,s^{-1}}$ and $U_{\mathrm{cloud}} = 6\,\mathrm{m\,s^{-1}}$. It follows that Δz_{sub} directly determines the wind shear ($\mathrm{d}U/\mathrm{d}z$), atmospheric stability ($\mathrm{d}\Theta_{\mathrm{l}}/\mathrm{d}z$) and, therefore, Ri. This dependency is demonstrated in Fig. 4 where the two gradients and Ri are shown to be approximately linear functions of Δz_{sub} (the gradients decreasing and Ri increasing).

The dependency of Ri on the square of the wind shear and linearly on temperature gradient (Eq. 1) directly leads to the question whether one can estimate a maximum thickness of the TIL. To first approximation both gradients decrease linearly with increasing TIL thickness, so the contribution of shear destabilization to the Richardson number decreases more rapidly than the stabilizing effect of temperature. A maximum thickness Δz_{max} should be reached when Ri exceeds the critical value of $Ri_{\mathrm{c}} \approx 1$. Approximating gradients with finite differences, Eq. 1 gives

$$\Delta z_{\mathrm{max}} \leq Ri_{\mathrm{c}}\,\frac{\overline{\Theta}_{\mathrm{l}}}{g}\,\frac{(\Delta U)^2}{\Delta\Theta_{\mathrm{l}}}, \tag{2}$$

where $\overline{\Theta}_{\mathrm{l}}$ represents the mean value in the TIL and $\Delta U = U_{\mathrm{top}} - U_{\mathrm{cloud}}$ and $\Delta\Theta_{\mathrm{l}} = \Theta_{\mathrm{l,top}} - \Theta_{\mathrm{l,cloud}}$. With the measurement results of $\overline{\Theta}_{\mathrm{l}} = 289\,\mathrm{K}$, $\Delta U = 5\,\mathrm{m\,s^{-1}}$ and $\Delta\Theta_{\mathrm{l}} = 8\,\mathrm{K}$ and an assumed $Ri_{\mathrm{c}} = 1$, a maximum thickness of $\Delta z_{\mathrm{max}} \approx 90\,\mathrm{m}$ is estimated. This estimate is consistent with the observed maximum of $\Delta z_{\mathrm{sub}} = 85\,\mathrm{m}$ (profile I in Fig. 1).

The corresponding picture is illustrated in Fig. 5. Figure 5a shows the idealized initial situation without the TIL and, therefore, infinite gradients of U and Θ_{l} at cloud top ($Sc\ top$) whereas Fig. 5b shows the situation after the TIL has developed and the gradients are finite. The layer is assumed to thicken until the critical Ri is achieved and further turbulent growth of the layer ceases due to decreasing shear. The situation is similar to the classical turbulent mixing layer, but in our case the fluid below the shear zone is turbulent and that above the shear zone is very weakly turbulent or quiescent. It could be considered the cloud-top

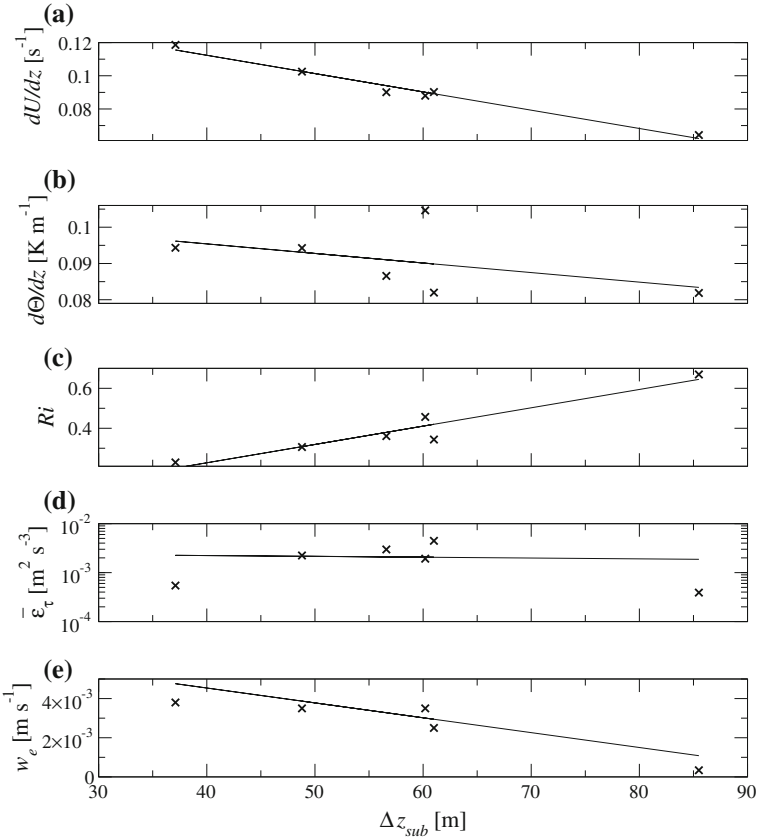

Fig. 4 Impact of the thickness (Δz_{sub}) of the TIL on its turbulent properties. Dependencies are calculated for: **a** horizontal wind shear ($\mathrm{d}U/\mathrm{d}z$), **b** atmospheric stability ($\mathrm{d}\theta/\mathrm{d}z$), **c** gradient Richardson number (Ri), **d** averaged local energy dissipation rate ($\overline{\varepsilon}_{\tau}$) and **e** entrainment velocity (w_{e})

analogue of the idealized, spatially localized shear layer discussed by Smyth and Moum (2000), for which "any initial stratification, however weak, will eventually prevail over the shear and damp the turbulence." The analogy is not perfect, however, because one half of the layer is constantly turbulent, and we speculate that this is the reason for the continuity of energy dissipation rate between the cloud layer and the TIL (e.g., see Figs. 2 and 3). Furthermore, these observations and the conceptual picture outlined in Fig. 5 are consistent with the LES studies of Brucker and Sarkar (2007) for a turbulent, stratified clear-air mixing layer and of Wang et al. (2008) for a stratocumulus top with strong shear, who both showed monotonic layer growth until $Ri \approx 0.3$.

At least semi-quantitatively, the TIL evolution can be further analyzed by considering the terms of the balance equation for turbulent kinetic energy (e.g., Brucker and Sarkar 2007):

$$\mathrm{d}E/\mathrm{d}t = P - B - \varepsilon = K_{\mathrm{m}} \left[\left(\frac{\Delta U}{\Delta z} \right)^2 - Pr \, \frac{g}{\Theta} \, \frac{\Delta \Theta}{\Delta z} \right] - \varepsilon. \tag{3}$$

Here the flux inside the buoyancy term (B) is approximated in terms of gradients, which can be approximated by the previously defined differences. We have neglected the transport

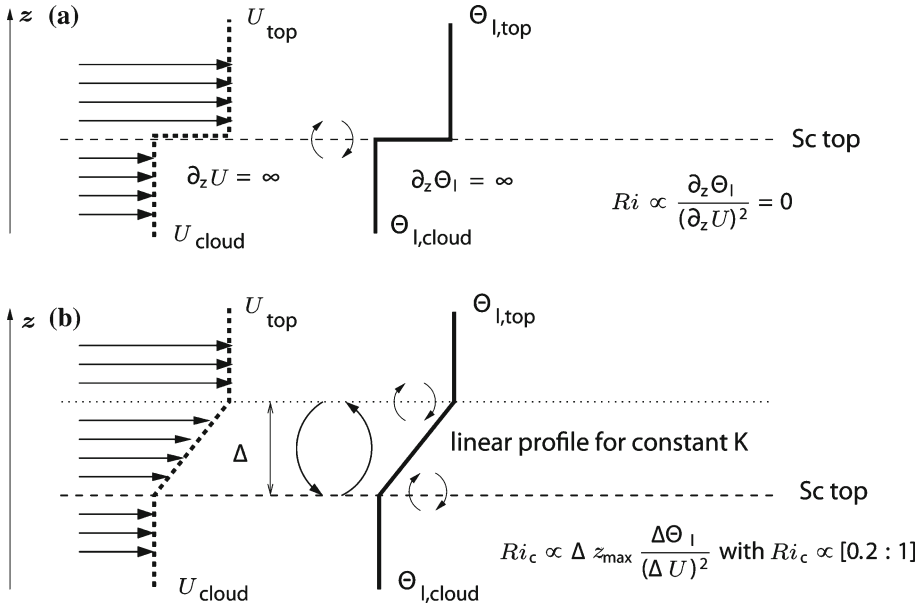

Fig. 5 Schematic illustration of the development of the cloud top due to entrainment. **a** Initial situation: between cloud layer (characterized by U_{cloud} and $\Theta_{\mathrm{l,cloud}}$) and free troposphere (characterized by U_{top} and $\Theta_{\mathrm{l,top}}$) an infinite inversion is located at *Sc top*. **b** Entrainment processes leads to the generation of a TIL within the inversion layer with a maximal thickness of Δz_{max}, which is determined by $\Delta\Theta_{\mathrm{l}}$, ΔU and the gradient Richardson number (see text for more details)

term, mainly because we are unable to make any reliable estimate of its contribution, but also with the logic that there is no strong vertical gradient of ε observed. Figure 6 shows the magnitude of the production (P) and buoyancy (B) terms as well as the difference $P - B$ and the observed mean ε. Here, the mean observed turbulent diffusion coefficient $K_{\mathrm{m}} \approx 0.2\,\mathrm{m^2\,s^{-1}}$ and again a Prandtl number $Pr \approx 1$ are used. For small Δz_{sub} the energy production due to shear dominates over the suppressing buoyancy, but with increasing Δz_{sub} the rate of increase of turbulent kinetic energy $\mathrm{d}E/\mathrm{d}t$ gradually decreases until a critical value of Δz is reached, beyond which $P - B$ becomes negative and turbulent kinetic energy is destroyed. Since ε is positive definite this is the maximum thickness to which the TIL can develop. For our observations this critical thickness is about 90 m, which corresponds well with the value estimated with the Richardson criterion and the maximum observed thickness (see previous paragraphs).

The influence of stratification on turbulence can be further elucidated by considering relative magnitudes of the large eddy scale ($l_{\mathrm{e}} = \sigma_{\mathrm{w}}^3/\varepsilon$), the Corrsin scale ($l_{\mathrm{c}} = \sqrt{\varepsilon/S^3}$) above which shear acts to distort eddies, and the Ozmidov scale ($l_{\mathrm{o}} = \sqrt{\varepsilon/N^3}$) above which buoyancy strongly influences the energetics (Smyth and Moum 2000). We find that these length scales are all on the order of 1 m (ranging from approximately 1 to 4 m) and that they do not change significantly or show any clear trend over the measured range of Δz_{sub}. Even within the scatter, however, it is observed that $l_{\mathrm{e}} > l_{\mathrm{o}} > l_{\mathrm{c}}$, confirming that the largest turbulent eddies are strongly influenced by buoyancy, as was initially indicated by the anisotropy in the large-scale velocity fluctuations (e.g., Figs. 2 and 3). But because l_{e} and l_{o} are of the same order of magnitude the majority of the turbulent cascade is likely not

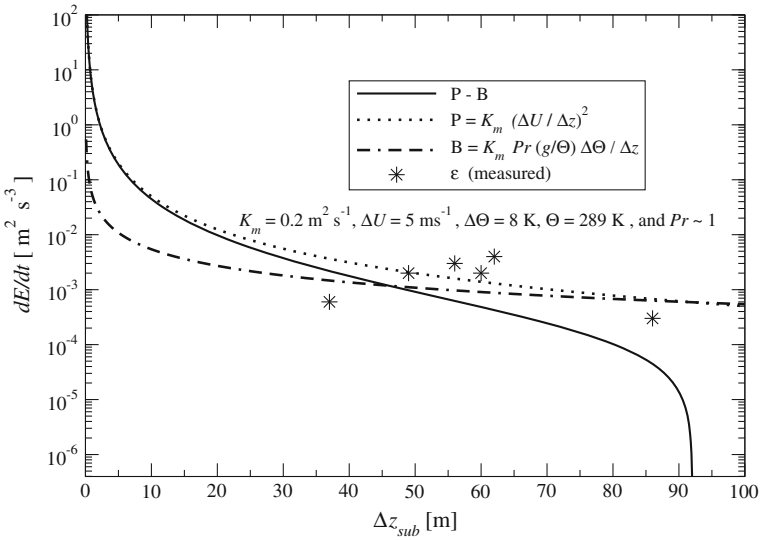

Fig. 6 Different terms of the turbulent kinetic energy balance equation, where P is the production due to shear, B is the buoyancy term and ε are observed energy dissipation rates as a function of TIL thickness Δz_{sub}. The values K_{m}, ΔU, $\Delta\Theta$ and mean Θ are from observations and Prandtl number $Pr \approx 1$ is assumed

strongly influenced by buoyancy effects. This is quantified by the ratio between the Ozmidov scale and the Kolmogorov scale ($l_{\mathrm{K}} = \left(\nu^3/\varepsilon\right)^{1/4}$) to give a buoyancy Reynolds number ($Re_{\mathrm{B}} = (l_{\mathrm{o}}/l_{\mathrm{K}})^{4/3} = \overline{\varepsilon}_\tau/(\nu N^2)$), of $4{,}500 < Re_{\mathrm{B}} < 65{,}000$. Such values are well beyond the critical value of $Re_{\mathrm{B}} = 20$ indicated by Smyth and Moum (2000) and indicate a large range of eddy scales unaffected by buoyancy and viscous dissipation damping effects. Even so, it should be noted that $l_{\mathrm{e}} \ll \Delta z_{\mathrm{sub}}$, and therefore the TIL is not thoroughly mixed by eddies of the same scale as the layer thickness, as might be the case for the underlying boundary layer, for example. This may account for the remarkably smooth, linear profiles observed even in instantaneous realizations of the TIL, as shown in Fig. 2.

The nearly linear profiles of mean Θ_{l}, a, U, and N inside the TIL, e.g., as shown in Figs. 2 and 3, are consistent with the assumption of constant turbulent diffusion coefficients K_{m} and K_{h} (for mass and heat, respectively). Therefore, a mean K_{m} can be calculated using the mixing length formulation suggested by Hanna (1968): $K_{\mathrm{m}} = 0.3\ \sigma_{\mathrm{w}}\ l = 0.3\ \sigma_{\mathrm{w}}^4\ \overline{\varepsilon}^{-1}$ with the typical large eddy length scale $l_{\mathrm{e}} = \sigma_{\mathrm{w}}^3/\overline{\varepsilon}$. For each profile, ε_τ is averaged over the TIL to estimate $\overline{\varepsilon}$. The standard deviation σ_{w} has been estimated from individually detrended segments of the profile with an integration length of 6 s each. The length has been chosen to interpret structures with a dimension up to about 12 m as turbulent fluctuations assuming a climbing rate of 2 m s^{-1}. Sensitivity tests with different integration lengths lead to a typical uncertainty for σ_{w} of about 10%; for one profile a maximum value of 25% was estimated. The range of the estimated l_{e} is 2–5 m resulting in a range for K_{m} of 0.1–0.3 m^2 s^{-1} for the six profiles.

Using K_{m} the entrainment flux can be approximated with the temperature gradient assuming $K_{\mathrm{m}} \approx K_{\mathrm{h}}$ (e.g., Prandtl number $Pr \approx 1$): $\overline{w'\Theta'} = -K_{\mathrm{h}}(\partial\Theta/\partial z) \approx -K_{\mathrm{h}}(\Delta\Theta/\Delta z_{\mathrm{sub}})$. Afterwards, the entrainment velocity can be calculated as $w_{\mathrm{e}} = (-\overline{w'\Theta'})/\Delta\Theta = K_{\mathrm{h}}/\Delta z_{\mathrm{sub}}$. The resulting entrainment velocities range from about 1 to 5×10^{-3} m s^{-1}, comparable for example to the values determined by Faloona et al. (2005) for the stratocumulus-topped

marine boundary layer. The dependences of $\overline{\varepsilon}_\tau$ and w_e on Δz_{sub} are shown in the two bottom panels of Fig. 4. Interestingly, the $\overline{\varepsilon}_\tau$ averaged over the TIL does not show a clear trend with Δz_{sub}. The estimated w_e, however, hints at a decrease with Δz_{sub}, which is consistent with the LES results of Wang et al. (2008). The decrease can be understood by noting that the entrainment velocity scales as $w_e \sim \sigma_w(l_e/\Delta z_{sub})$, and that l_e and σ_w are observed to be rather constant for the measured profiles. At least in the case of l_e, the lack of variability is likely due to its consistent collapse to be of the same order as l_o. If this is the case, it suggests that the ratio $l_e/\Delta z_{sub}$, already small, continues to decrease as the TIL thickens and that there is a minimum w_e corresponding to the maximum layer thickness Δz_{max} (i.e., when the critical Richardson number is reached). Therefore, we can speculate that, although the cloud interface is leaky to use the terminology of Lenschow et al. (2000), the leakiness decreases as the TIL develops. Furthermore, because $l_e/\Delta z_{sub} \ll 1$ we can qualitatively state that it likely grows through nibbling rather than engulfment. This effective elimination of direct communication between the cloud layer and the free troposphere may be the cause of the buffer against entrainment instability suggested by Rogers and Telford (1986).

The observations are for only one sampled boundary layer, but clouds sampled on other days show that the presence of a TIL is not an isolated event, and we therefore consider its possible general importance. First, this large-scale, shear-dominated situation contrasts with the picture of local-scale shear resulting from large-scale convective eddies (e.g., Sullivan et al. 1998; Kurowski et al. 2009). We can speculate that the large-scale convective eddies in this case are not so important in generating the shear, but possibly in driving vertical undulations that lead to variations in the TIL thickness. For example, one might envisage pulsating bursts of turbulence and entrainment as the boundary layer 'squeezes' the TIL and therefore sharpens the wind-shear gradient. This sharpening would lead, in turn, to a local reduction in Ri, analogous to that observed by Kurowski et al. (2009) in the weak shear scenario. In this view, while the mean vertical shear of horizontal wind speed is a property of the large-scale synoptic flow, the local thickness of the TIL itself is still coupled to boundary-layer dynamics, as is the local entrainment rate through its dependence on TIL thickness. One possible indication of such a squeezing effect could be the cloud top of profile II in Fig. 1 at a height of 1,286 m, while the cloud top of the neighbouring profiles is located at a height of 1,254 m. Furthermore, the thickness of the TIL of profile II is $\Delta z_{sub} = 37$ m, while the neighbouring TIL thickness are 85 m respectively 60 m. Clearly, more evidence would be necessary to support or refute this concept. For example, a consistent correlation between cloud-top height and TIL thickness could be indicative of a squeezing effect. Robust characterization of such a correlation would require measurements in an area with large-scale homogeneity, coupled with measurements of dynamics within the lower boundary layer. Second, properties of the TIL when it is present are relevant to the evolution of marine stratocumulus through the entrainment process. The TIL exists as a result of shear-induced entrainment of sub-saturated and potentially warmer free-tropospheric air. With increasing thickness of the TIL the air adjacent to the cloud top is increasingly cool and humid, so that local mixing events are less extreme in their thermodynamic properties as illustrated by the arrows indicating the eddies in Fig. 5. Thus, we can suppose that the microphysical response to cloud-top entrainment will undergo transition from inhomogeneous to more homogeneous mixing as the mixed air becomes increasingly 'pre-humidified' (Lehmann et al. 2009).

We have presented high spatial resolution measurements of thermodynamic, microphysical, and turbulence properties in the inversion layer at the top of marine stratocumulus clouds under conditions of strong vertical wind shear. The measurements were made with the ACTOS, which because of its low flight speed allows for relatively steep ascent or descent through the inversion and cloud-top layers, thereby minimizing horizontal averaging and

approaching instantaneous vertical profiles. The measurements reveal the presence of a layer of clear air above cloud top, characterized by nearly linear profiles of potential temperature, horizontal wind speed, absolute humidity, and aerosol concentration of interstitial aerosol. The layer is turbulent, with an energy dissipation rate nearly the same as that in the lower cloud, but with significant anisotropic turbulence at the large scales. We refer to this as the TIL. In six sampled profiles through the layer it is observed that the Richardson number increases with layer thickness to order unity, suggesting that the layer develops to the point where shear production of turbulence is sufficiently weak to be balanced by buoyancy suppression. This picture is consistent with the evolution of turbulence at localized stratified shear layers (Smyth and Moum 2000; Brucker and Sarkar 2007), and with the LES of Wang et al. (2008). The large eddy scale is suppressed by buoyancy to be on the order of the Ozmidov scale, much less than the thickness of the TIL, such that direct mixing between the cloud top and the free troposphere is inhibited. Indeed, the linear profiles in the layer can be considered indicative of turbulent diffusion with a constant linear eddy coefficient, allowing for estimation of the entrainment velocity, which apparently decreases with increasing TIL thickness.

Based on these observations and the resulting conceptual picture of a TIL, free of cloud, but diffusively connecting the cloud top to the free troposphere, we speculate that mean vertical shear of the horizontal air velocity is of primary importance in determining entrainment rates. The existence of turbulent mixing with a buoyancy-limited large eddy scale, and the resulting smooth gradients in thermodynamic properties through the TIL, may be the mechanism behind the buffering against cloud-top instability suggested by Rogers and Telford (1986). Subsequent work will be focused on the microphysical effects of mixing at cloud top, as a function of vertical shear.

Acknowledgments We acknowledge Rolf Maser and Dieter Schell from the enviscope GmbH (Frankfurt/M, Germany) for technical support and the two pilots Alwin Vollmer and Oliver Schubert from the rotorflug GmbH (Friedrichsdorf, Germany) for great helicopter flights. RAS acknowledges support from the Alexander von Humboldt Society during the period in which this research was carried out, as well as support from NSF grant AGS-1026123. We thank Don Lenschow, Szymon Malinowski, Juan-Pedro Mellado, and Bjorn Stevens for enlightening discussions about stratocumulus clouds.

References

Biltoft CA (2001) Some thoughts on local isotropy and the 4/3 lateral to longitudinal velocity spectrum ratio. Boundary-Layer Meteorol 100(3):393–404

Brucker KA, Sarkar S (2007) Evolution of an initially turbulent stratified shear layer. Phys Fluids 19:105105

Deardorff JW (1980) Cloud top entrainment instability. J Atmos Sci 37:131–147

de Roode SR, Wang Q (2007) Do stratocumulus clouds detrain? FIRE I data revisited. Boundary-Layer Meteorol 122(2):479–491

Faloona I, Lenschow DH, Campos T, Stevens B, van Zanten M, Blomquist B, Thornton D, Bandy A, Gerber H (2005) Observations of entrainment in eastern pacific marine stratocumulus using three conserved scalars. J Atmos Sci 62:3268–3285

Gerber H, Arends BG, Ackerman AS (1994) New microphysics sensor for aircraft use. Atmos Res 31(4): 235–252

Gerber H, Frick G, Malinowski SP, Brenguier JL, Burnet F (2005) Holes and entrainment in stratocumulus. J Atmos Sci 62(2):443–459

Haman KE, Makulski A, Malinowski SP, Busen R (1997) A new ultrafast thermometer for airborne measurements in clouds. J Atmos Oceanic Technol 14(2):217–227
Haman KE, Malinowski SP, Kurowski MJ, Gerber H, Brenguier JL (2007) Small scale mixing processes at the top of a marine stratocumulus—a case study. Q J Roy Meteorol Soc 133(622):213–226
Hanna SR (1968) A method of estimating vertical eddy transport in the planetary boundary layer using characteristics of the vertical velocity spectrum. J Atmos Sci 25:1026–1033
Kondo J, Kanechika O, Yasuda N (1978) Heat and momentum transfers under strong stability in the atmospheric surface layer. J Atmos Sci 35:1012–1021
Kurowski MJ, Malinowski SP, Grabowski WW (2009) A numerical investigation of entrainment and transport within a stratocumulus-topped boundary layer. Q J Roy Meteorol Soc 135(638):77–92
Lehmann K, Siebert H, Shaw RA (2009) Homogeneous and inhomogeneous mixing in cumulus clouds: dependence on local turbulence structure. J Atmos Sci 66(12):3641–3659
Lenschow D, Paluch I, Bandy A, Pearson R Jr, Kawa S, Weaver C, Huebert B, Kay J, Thornton D, Driedger A III (1988) Dynamics and chemistry of marine stratocumulus (DYCOMS) experiment. Bull Am Meteorol Soc 69:1058–1067
Lenschow DH, Zhou M, Zeng X, Chen L, Xu X (2000) Measurements of fine-scale structure at the top of marine stratocumulus. Boundary-Layer Meteorol 97(2):331–357
Mauritsen T, Svensson G, Zilitinkevich SS, Esau I, Enger L, Grisogono B (2007) A total turbulent energy closure model for neutrally and stably stratified atmospheric boundary layers. J Atmos Sci 64:4113–4126
Mellado JP (2010) The evaporatively driven cloud-top mixing layer. J Fluid Mech 660:5–36
Moeng CH, Stevens B, Sullivan PP (2005) Where is the interface of the stratocumulus-topped PBL?. J Atmos Sci 62(7):2626–2631
Peltier WR, Caulfield CP (2003) Mixing efficiency in stratified shear flows. Annu Rev Fluid Mech 35(1): 135–167
Rogers DP, Telford JW (1986) Metastable stratus tops. Q J Roy Meteorol Soc 112(472):481–500
Siebert H, Wendisch M, Conrath T, Teichmann U, Heintzenberg J (2003) A new tethered balloon-borne payload for fine-scale observations in the cloudy boundary layer. Boundary-Layer Meteorol 106(3):461–482
Siebert H, Franke H, Lehmann K, Maser R, Saw EW, Schell D, Shaw RA, Wendisch M (2006a) Probing fine-scale dynamics and microphysics of clouds with helicopter-borne measurements. Bull Am Meteorol Soc 87:1727–1738
Siebert H, Lehmann K, Wendisch M (2006b) Observations of small scale turbulence and energy dissipation rates in the cloudy boundary layer. J Atmos Sci 63:1451–1466
Siebert H, Shaw RA, Warhaft Z (2009) Statistics of small-scale velocity fluctuations and internal intermittency in marine stratocumulus clouds. J Atmos Sci 67:262–273
Smyth WD, Moum JN (2000) Length scales of turbulence in stably stratified mixing layers. Phys Fluids 12:1327–1342
Stevens B (2002) Entrainment in stratocumulus-topped mixed layers. Q J Roy Meteorol Soc 128(586):2663–2690
Sullivan PP, Moeng CH, Stevens B, Lenschow DH, Mayor SD (1998) Structure of the entrainment zone capping the convective atmospheric boundary layer. J Atmos Sci 55:3042–3064
Wang S, Golaz JC, Wang Q (2008) Effect of intense wind shear across the inversion on stratocumulus clouds. Geophys Res Lett 35:L15814
Wyngaard JC (2010) Turbulence in the atmosphere. Cambridge University Press, Cambridge, 408 pp